ADAPTIVE HYBRID FINITE ELEMENT/DIFFERENCE METHOD FOR MAXWELL'S EQUATIONS

LARISA BEILINA[1], MARCUS J. GROTE[2]

ABSTRACT. An explicit, adaptive, hybrid finite element/finite difference method is proposed for the numerical solution of Maxwell's equations in the time domain. The method is hybrid in the sense that different numerical methods, finite elements and finite differences, are used in different parts of the computational domain. Thus, we combine the flexibility of finite elements with the efficiency of finite differences. Furthermore, an a posteriori error estimate is derived for local adaptivity and error control inside the subregion, where finite elements are used. Numerical experiments illustrate the usefulness of computational adaptive error control of proposed new method.

Keywords: Maxwell's equations, hybrid finite element/finite difference method, adaptive finite element methods, a posteriori error estimates, efficiency, reliability.

AMS Subject Classification: 65M15, 65M32, 65M50

1. INTRODUCTION

The development of new more sophisticated algorithms for the numerical solution of Maxwell's equations is dictated by increasingly complex applications in electromagnetics. In 1966 Yee [40] introduced the first and probably most popular method, the Finite Difference Time Domain (FDTD) scheme, which is simple and efficient. However, the FDTD scheme can only be applied on structured (Cartesian) grids and suffers from the inaccurate representation of the solution on curved boundaries (staircase approximation) [7]. In contrast, Finite Element Methods (FEMs) can handle complex boundaries and unstructured grids. They also provide rigorous a posteriori error estimates which are useful for local adaptivity and error control. Yet FEMs are usually more expensive than the FDTD method, both in computer time and in memory requirement.

In many applications small scale features, such as geometric singularities or jumps in material coefficients, only occupy a small part of the computational domain, Ω. While the FDTD cannot be used in general in those regions where local refinement is needed, the use of a FEM everywhere throughout Ω, because of a few isolated regions, can be quite high a price to pay. Instead, hybrid schemes attempt to combine the advantages of the above two methods in a manner that retains the advantages of both, by using finite elements only where needed and employing the FDTD method everywhere else. In doing so, the computational domain Ω is divided into two subregions, Ω_{FDM} and Ω_{FEM}, corresponding to the FD and the FE regions, respectively, such that $\Omega = \Omega_{FDM} \cup \Omega_{FEM}$. These two regions are meshed using structured and triangular/tetrahedral meshes, respectively, with common nodes shared at the interface. Typically the unstructured region Ω_{FEM} is much smaller than Ω_{FDM}. It may consist of several disjoint components, where computations are independent of one another and easily performed in parallel; in particular, different finite elements can be used in different subdomains.

[1] Department of Mathematical Sciences, Chalmers University of Technology and Gothenburg University, SE-42196 Gothenburg, Sweden,
email: larisa@chalmers.se

[2] Department of Mathematics, University of Basel, CH–4051 Basel, Switzerland,
email:Marcus.Grote@unibas.ch

The FDTD method in Ω_{FDM} is standard. For the FE discretization of Maxwell's equations in Ω_{FEM}, however, different formulations are available. Examples are the edge elements of Nédélec [31], the node-based first-order formulation of Lee and Madsen [24, 27, 34], the Cartesian elements of Mur [30], the node-based curl-curl formulation with divergence condition of Paulsen and Lynch [32], and the node-based least-squares FEM by Jiang, Wu, and Povinelli [20] and also by Bergstrm [5]. Edge elements are probably the most satisfactory from a theoretical point of view [25]; in particular, they correctly represent singular behavior at reentrant corners. However, they are less attractive for time dependent computations, because the solution of a linear system is required at every time iteration. Indeed, in the case of triangular or tetrahedral edge elements, the entries of the diagonal matrix resulting from mass-lumping are not necessarily strictly positive [11]; therefore, explicit time stepping cannot be used in general. In contrast, nodal elements naturally lead to a fully explicit scheme when mass-lumping is applied [11, 23].

Even when the individual finite difference and finite element algorithms are stable, some instabilities can occur when the two methods are hybridized [28]. In early hybrid FEM/FDM schemes [39, 38] the inherent symmetry of the operators was lost at the interface between Ω_{FDM} and Ω_{FEM}, which indeed led to time instabilities; these instabilities were later treated by a combination of temporal filtering and frequency shifting [18]. Rylander and Bondeson [35, 36] and also Edelvik, Andersson and Ledfelt [9, 10] devised the first stable time-domain hybrid method, which combined FDTD on the structured part of the mesh with tetrahedral edge elements on the unstructured part – here the FDTD method is viewed as a FEM with edge elements on a hexahedral mesh, lumped through trapezoidal integration. By coupling hexahedra and tetrahedra with a layer of pyramids, an $H(\text{curl})$-conforming discretization of the electric field is obtained. To achieve stability in time, implicit time-stepping is nevertheless required inside Ω_{FEM}.

Various techniques are available to correctly represent field singularities at reentrant corners. Clearly, edge elements on a locally refined mesh can be used; alternatively, the singular field method [8] or the related singular complement method [1, 2] can be applied, too. Away from such isolated, well-defined, and predictable singularities, we seek a fully explicit hybrid FEM/FDM method for Maxwell's equations, where the FDTD method is used in the structured part and finite elements are used in the unstructured part of the mesh. Therefore we opt for node-based finite elements, which enable the use of mass-lumping in space and hence lead to in a fully explicit time integration scheme [23].

It is well known that numerical solutions of Maxwell's equations using nodal finite elements may contain spurious solutions [26, 32], and various techniques are available to remove them [19, 20, 21, 29, 32]. Following Paulsen and Lynch [32], we shall add a penalty term to enforce the divergence condition, which eliminates spurious solutions when combined with local mesh refinement.

The FEM not only handles unstructured grids for local refinement, but also offers the possibility for a posteriori error estimation, which enable automatic grid refinement, precisely where needed. Following Johnson et al. [14, 13, 15, 16, 22], we shall derive an a posteriori error estimate for the time dependent Maxwell equations, where the error is represented in terms of space-time integrals of the residuals of the computed solution multiplied by weights related to the solution of the dual problem. Inside Ω_{FEM} the finite element is then iteratively refined with feed-back from the a posteriori error estimation.

The outline of our work is as follows. In Section 2 we briefly recall Maxwell's equations. Then, in Section 3, we formulate the finite element method and discuss the problem of spurious solutions. The FDTD scheme is summarized in Section 4. Next, we formulate the hybrid FEM/FDM method in Section 5 and derive a posteriori error estimates. Finally, in Section 7 we present two- and three-dimensional time-dependent computations which demonstrate the effectiveness of our adaptive hybrid FEM/FDM solver.

2. Maxwell's equations

We consider Maxwell's equations in an inhomogeneous isotropic medium in a bounded domain $\Omega \subset \mathbb{R}^d$, $d = 2, 3$ with boundary Γ:

$$
\begin{aligned}
\frac{\partial D}{\partial t} - \nabla \times H &= -J, \text{ in } \Omega \times (0, T), \\
\frac{\partial B}{\partial t} + \nabla \times E &= 0, \text{ in } \Omega \times (0, T), \\
D &= \epsilon E, \\
B &= \mu H, \\
E(x, 0) &= E_0(x), \\
H(x, 0) &= H_0(x).
\end{aligned}
\tag{1}
$$

Here $E(x, t)$ and $H(x, t)$ are the (unknown) electric and magnetic fields, whereas $D(x, t)$ and $B(x, t)$ are the electric and magnetic inductions, respectively. The dielectric permittivity, $\epsilon(x) > 0$, and magnetic permeability, $\mu(x) > 0$, together with the current density, $J(x, t) \in \mathbb{R}^d$, are given and assumed piecewise smooth. Moreover, the electric and magnetic inductions satisfy the relations

$$
\nabla \cdot D = \rho, \ \nabla \cdot B = 0 \text{ in } \Omega \times (0, T),
\tag{2}
$$

where $\rho(x, t)$ is a given charge density. For simplicity, we restrict ourselves to perfectly conducting boundary conditions

$$
\begin{aligned}
E \times n &= 0, \text{ on } \Gamma \times (0, T), \\
H \cdot n &= 0, \text{ on } \Gamma \times (0, T),
\end{aligned}
\tag{3}
$$

where n is the outward normal on Γ. By eliminating B and D from (1) we obtain the two independent second order systems of partial differential equations

$$
\epsilon \frac{\partial^2 E}{\partial t^2} + \nabla \times (\mu^{-1} \nabla \times E) = -j,
\tag{4}
$$

$$
\mu \frac{\partial^2 H}{\partial t^2} + \nabla \times (\epsilon^{-1} \nabla \times H) = \nabla \times (\epsilon^{-1} J),
\tag{5}
$$

where $j = \frac{\partial J}{\partial t}$. The initial conditions are

$$
\begin{aligned}
E(x, 0) &= E_0, \tag{6} \\
H(x, 0) &= H_0, \tag{7} \\
\frac{\partial E}{\partial t}(x, 0) &= (\nabla \times H_0(x) - J(x, 0))/\epsilon(x), \tag{8} \\
\frac{\partial H}{\partial t}(x, 0) &= -\nabla \times E_0/\mu(x). \tag{9}
\end{aligned}
$$

From (4)-(9) we immediately infer that both E and H remain divergence-free for all time, if $\nabla \cdot E_0 = \nabla \cdot H_0 = \nabla \cdot J(., t) = 0$.

3. The finite element method

We shall use a hybrid finite element/finite difference method for the numerical solution of (4), (6) and (8). The method is hybrid in the sense that we shall use different numerical methods in different parts of the computational domain Ω. Let Ω separate into a finite element domain Ω_{FEM} and a finite difference domain Ω_{FDM}. We assume that Ω_{FEM} lies strictly inside Ω, that is away from the physical boundary Γ. It may consist of one or more subdomains and typically covers only a small part of Ω.

In Ω_{FDM} we shall use the finite difference Yee scheme [40] on a Cartesian equidistant mesh, which is based on the first order formulation of Maxwell's equations (1). In Ω_{FEM}, however, we shall use finite elements on a sequence of nondegenerate unstructured meshes $K_h = \{K\}$, with elements K consisting of triangles in $\mathbb{R}^2$ and tetrahedra in $\mathbb{R}^3$ [6]. Efficiency of the resulting scheme in Ω is obtained by using mass lumping in both space and time in Ω_{FEM}, which makes the scheme fully explicit [17]. In Ω_{FEM} we associate with K_h a (continuous) mesh function $h = h(x)$, which represents the diameter of the element K that contains x. For the time discretization we let $J_\tau = \{J\}$ be a partition of the time interval $I = [0, T]$, where $0 = t_0 < t_1 < ... < t_N = T$ is a sequence of discrete time steps with associated time intervals $J = (t_{k-1}, t_k]$ of constant length $\tau = t_k - t_{k-1}$.

3.1. **Finite element spaces.** When using standard, piecewise continuous $[H^1(\Omega)]^3$-conforming FE for the numerical solution of Maxwell's equations, one faces two difficulties. First, in general the solution of (4) lies in the space $H_0(\mathrm{curl}, \Omega) \cap H(\mathrm{div}, \Omega)$ with

$$H_0(\mathrm{curl}, \Omega) := \{u \in [L^2(\Omega)]^3 : \nabla \times u \in L^2(\Omega),\ u \times n = 0\}, \tag{10}$$

and

$$H(\mathrm{div}, \Omega) := \{u \in [L^2(\Omega)]^3 : \nabla \cdot u \in L^2(\Omega)\}; \tag{11}$$

here n is the unit outward normal to $\partial\Omega$. This space is strictly larger than $[H^1(\Omega)]^3$ when Ω has reentrant corners ([25], p.191). However, this restriction is of no concern here, because the FEM is used only in Ω_{FEM}, which lies strictly inside Ω; hence, corner singularities are excluded. Second, because the bilinear form $a(u, v) = (\nabla \times u, \nabla \times v)$ is not coercive without some (at least weak) restriction to divergence-free functions, direct application of the finite element method to the numerical solution of Maxwell's equations using $[H^1(\Omega)]^3$-conforming nodal finite elements can result in spurious solutions (the finite element solution does not satisfy the divergence condition (2)). To remove these spurious solutions from the finite element solution, we shall add a Coulomb-type gauge condition to enforce the divergence condition [3, 29, 32]. This approach is discussed in detail below.

3.2. **The problem of spurious solutions.** To remove spurious solutions from the finite element solution, we modify equations (4) - (5) following Paulsen and Lynch [32] as

$$\epsilon \frac{\partial^2 E}{\partial t^2} + \nabla \times (\mu^{-1} \nabla \times E) - s\nabla(\mu^{-1} \nabla \cdot E) - s\nabla(\nabla \cdot (-j)) = -j, \tag{12}$$

and

$$\mu \frac{\partial^2 H}{\partial t^2} + \nabla \times (\epsilon^{-1} \nabla \times H) - s\nabla(\epsilon^{-1} \nabla \cdot H) = \nabla \times (\epsilon^{-1} J), \tag{13}$$

respectively, where $s > 0$ denotes the penalty factor. Since the (modified) bilinear form $a(u, v) = (\nabla \times u, \nabla \times v) + s(\nabla \cdot u, \nabla \cdot v)$ is coercive on $[H^1(\Omega)]^3$ for any $s > 0$, both initial-boundary value problems (12) and (13), with initial conditions (6) - (9), are now well-posed; hence, in the continuous setting value of $s > 0$ is irrelevant. The addition of the term $s(\nabla \cdot u, \nabla \cdot v)$ does not change either solution of (12), (13), but only provides a stabilization of the variational formulation - see also ([25], p.191). However, on a fixed mesh with given parameters μ, ϵ, the value of s determines the emphasis one places on the gauge condition. Too small a value of s can give rise of spurious solutions, which will vanish as $h \to 0$. In practice, a good choice is $s = 1$ [21, 32].

3.3. **The finite element method.** For simplicity, we now restrict ourselves to the finite element formulation of (12) together with the initial conditions

$$\frac{\partial E}{\partial t}(x, 0) = E(x, 0) = 0, \tag{14}$$

and perfectly conducting boundary condition

$$E \times n = 0. \tag{15}$$

To formulate a finite element method for (12), (14), and (15) we introduce the finite element trial space W_h^E, defined by

$$W_h^E := \{w \in W^E : w|_{K \times J} \in [P_1(K) \times P_1(J)]^3, \forall K \in K_h, \forall J \in J_\tau\},$$

where $P_1(K)$ and $P_1(J)$ denote the set of linear functions on K and J, respectively, and

$$W^E := \{w \in [H^1(\Omega \times I)]^3 : w(\cdot, 0) = 0, w \times n|_\Gamma = 0\}.$$

Hence, the finite element space W_h^E consists of continuous piecewise linear functions in space and time, which satisfy certain homogeneous initial and boundary conditions. We also define the following L_2 inner products and norms

$$((p, q)) = \int_\Omega \int_0^T pq \, dx \, dt, \quad \|p\|^2 = ((p, p)),$$

$$(\alpha, \beta) = \int_\Omega \alpha\beta \, dx, \quad |\alpha|^2 = (\alpha, \alpha).$$

The finite element method for (12) now reads: Find $E_h \in W_h^E$ such that $\forall \bar\varphi \in W_h^E$,

$$\begin{aligned}
&- ((\epsilon \frac{\partial E_h^k}{\partial t}, \frac{\partial \bar\varphi}{\partial t})) + ((j^k, \bar\varphi)) + \\
&+ ((\frac{1}{\mu}\nabla \times E_h^k, \nabla \times \bar\varphi)) + s((\frac{1}{\mu}\nabla \cdot E_h^k, \nabla \cdot \bar\varphi)) - s((\frac{1}{\mu}\nabla \cdot j^k, \nabla \cdot \bar\varphi)) = 0.
\end{aligned} \tag{16}$$

Here, the initial condition $\frac{\partial E}{\partial t}(x, 0) = 0$ and the perfectly conducting boundary condition (15) are imposed weakly through the variational formulation.

3.4. **The explicit scheme for the electric field.** We expand E in terms of the standard continuous piecewise linear functions in space and in time and substitute E in (16). This yields the linear system of equations:

$$M(\mathbf{E}^{k+1} - 2\mathbf{E}^k + \mathbf{E}^{k-1}) = -\tau^2 F^k + s\tau^2 C\mathbf{j}^k - \tau^2 K\mathbf{E}^k - s\tau^2 C\mathbf{E}^k, \tag{17}$$

with initial conditions $\mathbf{E}^0$ and $\mathbf{E}^1$ set to zero because of (14). Here, M is the block mass matrix in space, K is the block stiffness matrix corresponding to the curl term, C is the stiffness matrix corresponding to the divergence term, F^k is the load vector at time level t_k corresponding to $j(\cdot, \cdot)$, whereas $\mathbf{E}^k$ and $\mathbf{j}^k$ denote the nodal values of $E(\cdot, t_k)$ and $j(\cdot, t_k)$, respectively.

At the element level the matrix entries in (17) are explicitly given by:

$$M_{i,j}^e = (\epsilon \, \varphi_i, \varphi_j)_e, \tag{18}$$

$$K_{i,j}^e = (\frac{1}{\mu} \, \nabla \times \varphi_i, \nabla \times \varphi_j)_e, \tag{19}$$

$$C_{i,j}^e = (\frac{1}{\mu} \, \nabla \cdot \varphi_i, \nabla \cdot \varphi_j)_e, \tag{20}$$

$$F_{j,m}^e = ((j, \varphi_j \psi_m))_{e \times J}. \tag{21}$$

To obtain an explicit scheme we approximate M by the lumped mass matrix M^L, i.e., the diagonal approximation obtained by taking the row sum of M [17, 23]. By multiplying (17) with $(M^L)^{-1}$, we obtain the following fully explicit time stepping method:

$$\begin{aligned}
\mathbf{E}^{k+1} = &- \tau^2 (M^L)^{-1} F^k + 2\mathbf{E}^k - \tau^2 (M^L)^{-1} K\mathbf{E}^k - \\
&- s\tau^2 (M^L)^{-1} C\mathbf{E}^k + s\tau^2 (M^L)^{-1} C\mathbf{j}^k - \mathbf{E}^{k-1}.
\end{aligned} \tag{22}$$

4. The finite difference method

4.1. **Finite difference formulation.** Here we briefly recall the Yee scheme [40] for the finite difference discretization of the time-dependent Maxwell equations (1) in three dimensions. The FDTD method is based on centered finite difference approximations of the first order derivatives in (1) on staggered grids, both in time and space, which results in a second order scheme. A typical update for the first components of the magnetic and electric fields - ϵ, μ are assumed constant for simplicity - takes the form

$$
\begin{aligned}
H_{1}{}^{n+\frac{1}{2}}_{p,q+\frac{1}{2},r+\frac{1}{2}} = H_{1}{}^{n-\frac{1}{2}}_{p,q+\frac{1}{2},r+\frac{1}{2}} - \\
- \frac{\tau}{\mu}\left(\frac{E_{3}{}^{n}_{p,q+1,r+\frac{1}{2}} - E_{3}{}^{n}_{p,q,r+\frac{1}{2}}}{\triangle y} - \frac{E_{2}{}^{n}_{p,q+\frac{1}{2},r+1} - E_{2}{}^{n}_{p,q+\frac{1}{2},r}}{\triangle z}\right),
\end{aligned} \tag{23}
$$

$$
\begin{aligned}
E_{1}{}^{n+1}_{p+\frac{1}{2},q,r} = E_{1}{}^{n}_{p+\frac{1}{2},q,r} - \frac{\tau}{\epsilon}J_{1}{}^{n+\frac{1}{2}}_{p+\frac{1}{2},q,r} + \\
+ \frac{\tau}{\epsilon}\left(\frac{H_{3}{}^{n+\frac{1}{2}}_{p+\frac{1}{2},q+\frac{1}{2},r} - H_{3}{}^{n+\frac{1}{2}}_{p+\frac{1}{2},q-\frac{1}{2},r}}{\triangle y} - \frac{H_{2}{}^{n+\frac{1}{2}}_{p+\frac{1}{2},q,r+\frac{1}{2}} - H_{2}{}^{n+\frac{1}{2}}_{p+\frac{1}{2},q,r-\frac{1}{2}}}{\triangle z}\right).
\end{aligned} \tag{24}
$$

Here $\triangle x$, $\triangle y$, and $\triangle z$ denote the spatial mesh sizes underlying the finite difference discretization. The corresponding equations for E_2, E_3, H_2 and H_3 are obtained by cyclic permutation of the indices for the various electromagnetic field components E_i and H_i, $i = 1, 2, 3$ - see [37] or [40] for further details.

4.2. **Dispersion relation and stability.** We now recall the dispersion relation for the Yee scheme, when applied to (1), with $j = 0$. Thus, we look for discrete plane wave solutions of (23) - (24) in the form

$$
\begin{aligned}
E(x, y, z, t) = E_0 e^{i(\omega t + k_1 \triangle x + k_2 \triangle y + k_3 \triangle z)}, \ E_0 \in \mathbb{R}^3, \\
H(x, y, z, t) = H_0 e^{i(\omega t + k_1 \triangle x + k_2 \triangle y + k_3 \triangle z)}, \ H_0 \in \mathbb{R}^3.
\end{aligned} \tag{25}
$$

For instance, by substituting (25) into (24) for E_1, we obtain:

$$
\begin{aligned}
\frac{\epsilon}{\tau}E_{01}\big(e^{i((n+1)\omega\tau + (p+\frac{1}{2})k_1\triangle x + qk_2\triangle y + rk_3\triangle z)} - \\
- e^{i(n\omega\tau + (p+\frac{1}{2})k_1\triangle x + qk_2\triangle y + rk_3\triangle z)}\big) + \\
+ \frac{H_{02}}{\triangle z}\big(e^{i((n+\frac{1}{2})\omega\tau + (p+\frac{1}{2})k_1\triangle x + qk_2\triangle y + (r+\frac{1}{2})k_3\triangle z)} - \\
- e^{i((n+\frac{1}{2})\omega\tau + (p+\frac{1}{2})k_1\triangle x + qk_2\triangle y + (r-\frac{1}{2})k_3\triangle z)}\big) - \\
- \frac{H_{03}}{\triangle y}\big(e^{i((n+\frac{1}{2})\omega\tau + (p+\frac{1}{2})k_1\triangle x + (q+\frac{1}{2})k_2\triangle y + rk_3\triangle z)} - \\
- e^{i((n+\frac{1}{2})\omega\tau + (p+\frac{1}{2})k_1\triangle x + (q-\frac{1}{2})k_2\triangle y + rk_3\triangle z)}\big) = 0.
\end{aligned} \tag{26}
$$

Next, we divide (26) by $e^{i((n+\frac{1}{2})\omega\tau + (p+\frac{1}{2})k_1\triangle x + qk_2\triangle y + rk_3\triangle z)}$ and iterate this process for the other components of the electric and magnetic fields. These calculations yield the following linear system:

$$
\begin{aligned}
\sin\frac{\omega\tau}{2}E_0 = \mathbf{C_1}H_0, \\
\sin\frac{\omega\tau}{2}H_0 = \mathbf{C_2}E_0,
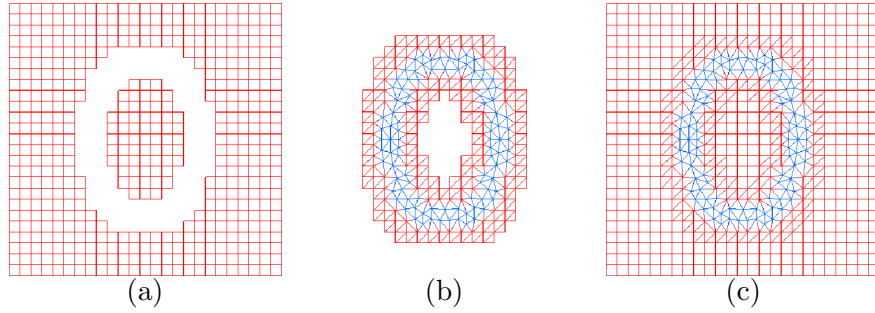\end{aligned} \tag{27}
$$

FIGURE 1. Domain decomposition. The hybrid mesh (c) is a combination of the structured mesh Ω_{FDM} (a) and the unstructured mesh Ω_{FEM} (b), with a thin overlap of structured elements. Here the unstructured grid is constructed so that the grid contains edges approximating an ellipse.

where both $\mathbf{C_1} = \frac{\tau}{\epsilon}\mathbf{C}$ and $\mathbf{C_2} = \frac{\tau}{\mu}\mathbf{C}$ are 3×3 matrices with

$$\mathbf{C} = \begin{pmatrix} 0 & -\sin(k_3\triangle z/2)/\triangle z & -\sin(k_2\triangle y/2)/\triangle y \\ \sin(k_3\triangle z/2)/\triangle z & 0 & -\sin(k_1\triangle x/2)/\triangle x \\ -\sin(k_2\triangle y/2)/\triangle y & \sin(k_1\triangle x/2)/\triangle x & 0 \end{pmatrix}.$$

Next, we eliminate H_0 from (27) by inserting the second equation into the first, which yields the following 3×3 eigenvalue problem

$$\sin^2\frac{\omega\tau}{2}E_0 = \mathbf{C_1}\mathbf{C_2}E_0, \tag{28}$$

with eigenvalue $\sin^2\frac{\omega\tau}{2}$ and eigenvector E_0. Finally, from (28) we derive the dispersion relation

$$\sin^2\frac{\omega\tau}{2} = \frac{\tau^2}{\epsilon\mu}\Big(\sin^2(k_1\triangle x/2)/\triangle x^2 + \sin^2(k_2\triangle y/2)/\triangle y^2 + \sin^2(k_3\triangle z/2)/\triangle z^2\Big). \tag{29}$$

We apply a standard von Neumann stability analysis to determine the largest time step τ, for which the finite difference scheme remains stable. Thus, we require $|\sin\frac{\omega\tau}{2}| \leq 1$ for all discrete Fourier modes resolved on the grid and, in particular, for the highest spatial frequencies given by $k_1\triangle x = k_2\triangle y = k_3\triangle z = \pi$. This yields the stability condition

$$\tau \leq \frac{\sqrt{\epsilon\mu}}{\sqrt{\frac{1}{\triangle x^2} + \frac{1}{\triangle y^2} + \frac{1}{\triangle z^2}}}. \tag{30}$$

5. THE HYBRID METHOD

We now describe the data communication between the finite element method on the unstructured part of the mesh, Ω_{FEM}, and the finite difference method on the structured part, Ω_{FDM}. In practice, the communication is achieved by mesh overlapping across a two-element thick layer around Ω_{FEM} - see Fig. 2.

Next, we will formulate the hybrid method, which uses a hybrid discretization of the computational domain, as shown in Fig. 2. First, we observe that the interior nodes of the computational domain belong to either of the following sets:

ω_o: Nodes 'o' interior to Ω_{FDM} that lie on the boundary of Ω_{FEM},
$\omega_\times$: Nodes '×' interior to Ω_{FEM} that lie on the boundary of Ω_{FDM},
ω_*: Nodes '*' interior to Ω_{FEM} that are not contained in Ω_{FDM},
ω_D: Nodes 'D' interior to Ω_{FDM} that are not contained in Ω_{FEM}.
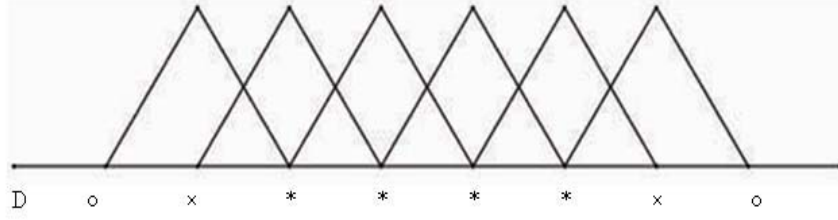
FIGURE 2. Coupling between FEM and FDM in one dimension. The interior nodes of the unstructured FEM grid are denoted by stars, while circles and crosses denote nodes, which are shared between the FEM and FDM grids. The circles are interior nodes of the FDM grid, while the crosses are interior nodes of the FEM grid. At each time iteration, FDM solution values at circles are copied to the corresponding FEM solution values, while simultaneously the FEM solution values are copied to the corresponding FDM solution values at cross nodes.

Algorithm. In our algorithm, nodes belonging to ω_o and $\omega_\times$ are stored twice, as nodes belonging to both Ω_{FEM} and Ω_{FDM}. At every time step we perform the following operations:

(1) On the structured part of the mesh Ω_{FDM} compute $H^{n+\frac{1}{2}}$, with $H^{n-\frac{1}{2}}$ known, and then compute E^{n+1} from (24), with E^n known and $H^{n+\frac{1}{2}}$ given by (23).

(2) On the unstructured part of the mesh Ω_{FEM} compute E^{n+1} by using the explicit finite element scheme (22).

(3) Use the values of the electric field E at nodes $\omega_\times$ as a boundary condition for the finite difference method in Ω_{FDM}. To get the values of E_1 at nodes $\omega_\times$ for the finite difference method, we use the following approximation:

$$E_{1_{FDM}}\left(p + \frac{1}{2}, q, r\right) = \frac{E_{1_{FEM}}(p+1, q, r) + E_{1_{FEM}}(p, q, r)}{2}. \tag{31}$$

All other components of the electric field are obtained similarly.

(4) Use the values of the electric field E at nodes ω_o as a boundary condition for the finite element method in Ω_{FEM}. The following approximation is used to get the values of E_1 at nodes ω_o:

$$E_{1_{FEM}}(p, q, r) = \frac{E_{1_{FDM}}\left(p + \frac{1}{2}, q, r\right) + E_{1_{FDM}}\left(p - \frac{1}{2}, q, r\right)}{2}. \tag{32}$$

The remaing components $E_{2_{FEM}}, E_{3_{FEM}}$ are obtained similarly.

6. A POSTERIORI ERROR ANALYSIS

Following previous works of Johnson and co-workers [13, 15, 16], we now present the main steps leading to an adaptive error control strategy, which is based on representing the error in terms of the solution of the adjoint, or dual problem. We shall first recall the general strategy for deriving a posteriori error estimates in an abstract framework. A posteriori error bounds for (12) are then derived in detail in Section 6.1.

Let us rewrite equation (12) as an error equation for the error $e = E - E_h$

$$Ae := \epsilon \frac{\partial^2 e}{\partial t^2} + \nabla \times (\mu^{-1}\nabla \times e) - s\nabla(\mu^{-1}\nabla \cdot e) - s\nabla(\nabla \cdot (-j)) = -j,$$
$$e \times n = 0 \text{ on } \Gamma,$$
$$e(\cdot, T) = 0 \text{ in } \Omega, \tag{33}$$
$$\frac{\partial e}{\partial t}(\cdot, T) = 0 \text{ in } \Omega.$$

Then we define the adjoint operator A^* to the operator A as

$$A^*\varphi := \epsilon\frac{\partial^2\varphi}{\partial t^2} + \nabla \times (\mu^{-1}\nabla \times \varphi) - s\nabla(\mu^{-1}\nabla \cdot \varphi) = e \text{ in } \Omega \times (0,T),$$

$$\varphi \times n = 0 \text{ on } \Gamma,$$

$$\varphi(\cdot,T) = 0 \text{ in } \Omega, \tag{34}$$

$$\frac{\partial\varphi}{\partial t}(\cdot,T) = 0 \text{ in } \Omega.$$

We have now following error representation formula

$$||e||^2_{L_2} = (e, A^*\varphi) = (Ae, \varphi) = (R, \varphi),$$

where $R = -j - Ae$ is the residual.

Next, we use the splitting

$$\varphi - \varphi_h = (\varphi - \varphi_h^I) + (\varphi_h^I - \varphi_h),$$

where $\varphi_h^I \in U_h$ denotes an interpolant of φ, together with Galerkin orthogonality

$$(R, \varphi_h^I - \varphi_h) = 0 \ \forall\varphi_h^I - \varphi_h \in U_h.$$

This finally yields the following error representation:

$$||e||^2_{L_2} \leq (R, \varphi - \varphi_h^I), \tag{35}$$

with $\varphi - \varphi_h^I$ appearing as a weight. Then we combine the standard interpolation estimates

$$||\varphi - \varphi_h^I||_{L_2} \leq (h^2 + \tau^2)C_i||D^2\varphi||_{L_2} \tag{36}$$

with interpolation constant C_i, together with strong stability estimate for the dual problem

$$||D^2\varphi||_{L_2} \leq C_s||e||_{L_2} \tag{37}$$

with stability constant C_s and get following a posteriori error estimate

$$||e||_{L_2} \leq C_iC_s(h^2 + \tau^2)||R||. \tag{38}$$

We now explicitly apply this general approach to the time dependent Maxwell equations.

6.1. **A posteriori error estimation for Maxwell's equations.** The a posteriori error analysis is based on representing the error in terms of the solution φ of the adjoint, or dual problem, related to (12). Thus, we wish to control the quantity $((e, \psi))$ with $e = E - E_h$ in $\Omega \times (0,T)$, where $\psi \in [H^1(\Omega \times I)]^3$ is given.

For the dual solution we introduce the finite element test space W_h^φ defined by:

$$W_h^\varphi := \{w \in W^\varphi : w|_{K\times J} \in P_1(K) \times P_1(J), \forall K \in K_h, \forall J \in J_\tau\},$$

where

$$W^\varphi := \{w \in H^1(\Omega \times I) : w(\cdot,T) = 0, w \times n|_\Gamma = 0\}.$$

The dual problem for (12) reads: find $\varphi \in W_h^\varphi$ such that

$$\epsilon\frac{\partial^2\varphi}{\partial t^2} + \nabla \times (\mu^{-1}\nabla \times \varphi) - s\nabla(\mu^{-1}\nabla \cdot \varphi) = \psi \text{ in } \Omega \times (0,T),$$

$$\varphi \times n = 0 \text{ on } \Gamma,$$

$$\varphi(\cdot,T) = 0 \text{ in } \Omega, \tag{39}$$

$$\frac{\partial\varphi}{\partial t}(\cdot,T) = 0 \text{ in } \Omega.$$

To begin we write the equation for the error as

$$\int_0^T \int_\Omega e\psi \ dx \ dt = \int_0^T \int_\Omega e\psi \ dxdt+$$

$$+ \int_0^T \int_\Omega e(\epsilon \frac{\partial^2 \varphi}{\partial t^2} + \nabla \times (\mu^{-1}\nabla \times \varphi) - s\nabla(\mu^{-1}\nabla \cdot \varphi) - \psi) \ dx \ dt = \tag{40}$$

$$= \int_0^T \int_\Omega e(\epsilon \frac{\partial^2 \varphi}{\partial t^2} + \nabla \times (\mu^{-1}\nabla \times \varphi) - s\nabla(\mu^{-1}\nabla \cdot \varphi)) \ dx \ dt.$$

Next, we integrate by parts twice the last term in (40), using that $\varphi(\cdot,T) = \frac{\partial \varphi}{\partial t}(\cdot,T) = 0, E(\cdot,0) = \frac{\partial E}{\partial t}(\cdot,0) = 0$ and $\varphi \times n = E \times n = 0$ on Γ. This yields:

$$-\int_0^T \int_\Omega \epsilon \frac{\partial e}{\partial t} \frac{\partial \varphi}{\partial t} \ dx \ dt + \int_0^T \int_\Omega (\mu^{-1}\nabla \times \varphi)(\nabla \times e) \ dx \ dt+$$

$$+s\int_0^T \int_\Omega (\mu^{-1}\nabla \cdot \varphi)(\nabla \cdot e) \ dx \ dt + \sum_k \int_\Omega \epsilon \left[\frac{\partial \varphi}{\partial t}(t_k)\right] e(t_k) \ dx+$$

$$+\sum_K \int_0^T \int_{\partial K} (\frac{1}{\mu}\nabla \times \varphi)(e \times n_K) \ dsdt + s\sum_K \int_0^T \int_{\partial K} (\frac{1}{\mu}\nabla \cdot \varphi)(e \cdot n_K) \ dsdt =$$

$$= \int_0^T \int_\Omega \left(\epsilon \frac{\partial^2 e}{\partial t^2} + \nabla \times (\mu^{-1}\nabla \times e) - s\nabla(\mu^{-1}\nabla \cdot e)\right)\varphi \ dx \ dt+ \tag{41}$$

$$+\sum_k \int_\Omega \epsilon \left[\frac{\partial \varphi}{\partial t}(t_k)\right] e(t_k) \ dx + \sum_K \int_0^T \int_{\partial K} (\frac{1}{\mu}\nabla \times \varphi)(e \times n_K) \ dsdt+$$

$$+s\sum_K \int_0^T \int_{\partial K} (\frac{1}{\mu}\nabla \cdot \varphi)(e \cdot n_K) \ dsdt - \sum_k \int_\Omega \epsilon \left[\frac{\partial e}{\partial t}(t_k)\right]\varphi(t_k) \ dx-$$

$$-\sum_K \int_0^T \int_{\partial K} \mu^{-1}\left(n_K \times \nabla \times e\right)\varphi \ dsdt + s\sum_K \int_0^T \int_{\partial K} (\mu^{-1}\nabla \cdot e)(n_K \cdot \varphi) \ ds \ dt =$$

$$= I_1 + I_2 + I_3 + I_4 + I_5 + I_6 + I_7,$$

where $I_i, \ i = 1,...,7$ denote the seven integrals that appear on the right of (41). In particular, I_3, I_4, I_6 and I_7 result from integration by parts in space, whereas $\left[\frac{\partial e}{\partial t}\right]$ and $\left[\frac{\partial \varphi}{\partial t}\right]$, the jumps in time of $\frac{\partial e}{\partial t}$ and $\frac{\partial \varphi}{\partial t}$, respectively, at time t_k which result from integration by parts in time.

In I_3 we sum over the element boundaries, where each internal side $S \in S_h$ occurs twice. Let e_s denote the function e in one of the normal directions of each side S. Then we can write I_3 as

$$\sum_K \int_{\partial K} (\frac{1}{\mu}e \times n_K)(\nabla \times \varphi) \ ds = \sum_S \int_S \frac{1}{\mu}\left[e_s \times n\right] \nabla \times \varphi \ ds, \tag{42}$$

where $\left[e_s \times n\right]$ denotes the jump in e across the two elements sharing S. We distribute each jump equally between the two neighboring elements and rewrite the sum over all element edges ∂K as :

$$\sum_S \int_S \frac{1}{\mu}\left[e_s \times n\right] \nabla \times \varphi \ ds = \sum_K \frac{1}{2}h_K^{-1}\int_{\partial K} \frac{1}{\mu}\left[e_s \times n\right] \nabla \times \varphi \ h_K \ ds. \tag{43}$$

Next, we formally set $dx = h_K ds$ and replace the integrals over the element boundaries ∂K by integrals over the elements K. Thus, we find:

$$\left|\sum_K \frac{1}{2}h_K^{-1}\int_{\partial K} \frac{1}{\mu}\left[e_s \times n\right] \nabla \times \varphi \ h_K \ ds\right| \leq C \int_\Omega \max_{S \subset \partial K} h_K^{-1}\frac{1}{\mu}\left|\left[e_s \times n\right]\right| \cdot \left|\nabla \times \varphi\right| \ dx, \tag{44}$$

with $\left[e_s \times n\right]\big|_K = \max_{S \subset \partial K} \left[e_s \times n\right]\big|_S$. Here and below we denote by C various positive constants of moderate size. In a similar way we estimate the jump in time in I_2 and I_5 by
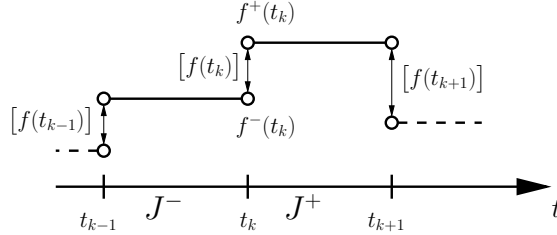

FIGURE 3. The jump in time of a function f.

multiplying and dividing by step size in time τ. More precisely, for estimation I_2 we have

$$\left| \sum_k \int_\Omega \epsilon \left[\frac{\partial \varphi}{\partial t}(t_k) \right] e(t_k) \, dx \right| \leq \sum_k \int_\Omega \epsilon \tau^{-1} \left| \left[\frac{\partial \varphi}{\partial t}(t_k) \right] \right| \left| e(t_k) \right| \tau dx \leq$$
$$\leq C \sum_k \int_{J_k} \int_\Omega \epsilon \tau^{-1} \left| \left[\partial_{t_k} \varphi \right] \right| \left| e(t_k) \right| \, dx dt = C \epsilon \tau^{-1} \int_0^T \int_\Omega \left| \left[\partial_{t_k} \varphi \right] \right| \cdot \left| e(t_k) \right| dx dt. \tag{45}$$

Here, we have defined $[\partial_{t_k} \varphi]$ as the greatest of the two jumps on the interval $J_k = (t_k, t_{k+1}]$:

$$[\partial_{t_k} \varphi] = \max_{J_k} \left(\left[\frac{\partial \varphi}{\partial t}(t_k) \right], \left[\frac{\partial \varphi}{\partial t}(t_{k+1}) \right] \right),$$

where

$$\left[\frac{\partial \varphi}{\partial t}(t_k) \right] = \frac{\partial \varphi}{\partial t}^+ (t_k) - \frac{\partial \varphi}{\partial t}^- (t_k).$$

The time jumps are illustrated in Figure 3.

Using Galerkin orthogonality (16) we substitute the above expressions into (41) with $e = E - E_h$, where we recognize $-j - s\nabla(\nabla \cdot j) = \epsilon \frac{\partial^2 E}{\partial t^2} + \nabla \times (\mu^{-1}\nabla \times E) - s\nabla(\mu^{-1}\nabla \cdot E)$, to get:

$$\int_0^T \int_\Omega \left| e \right| \left| \psi \right| \, dx \, dt \leq \int_0^T \int_\Omega \left| - j - s\nabla(\nabla \cdot j) - \epsilon \frac{\partial^2 E_h}{\partial t^2} - \nabla \times (\mu^{-1}\nabla \times E_h) + \right.$$
$$\left. + s\nabla(\mu^{-1}\nabla \cdot E_h) \right| \cdot \left| \varphi \right| \, dx \, dt +$$
$$+ C \int_0^T \int_\Omega \epsilon \cdot \left| \left[\partial_{t_k} \varphi \right] \right| \cdot \left| E_h \right| \, dx \, dt +$$
$$+ C \int_0^T \int_\Omega \max_{S \subset \partial K} h_K^{-1} \frac{1}{\mu} \left| \left[E_h \times n \right] \right| \cdot \left| \nabla \times \varphi \right| \, dx \, dt +$$
$$+ C \int_0^T \int_\Omega \max_{S \subset \partial K} h_K^{-1} \frac{1}{\mu} \left| \left[E_h \cdot n \right] \right| \cdot \left| \nabla \cdot \varphi \right| \, dx \, dt + \tag{46}$$
$$+ C \int_0^T \int_\Omega \epsilon \cdot \left| \left[\partial_{t_k} E_h \right] \right| \cdot \left| \varphi \right| \, dx \, dt +$$
$$+ C \int_0^T \int_\Omega \max_{S \subset \partial K} h_K^{-1} \frac{1}{\mu} \left| \left[n \times \nabla \times E_h \right] \right| \cdot \left| \varphi \right| \, dx \, dt +$$
$$+ C \int_0^T \int_\Omega \max_{S \subset \partial K} h_K^{-1} \frac{1}{\mu} \left| \left[n \cdot \varphi \right] \right| \cdot \left| \nabla \cdot E_h \right| \, dx \, dt.$$

We then introduce the splitting $\varphi - \varphi_h = (\varphi - \varphi_h^I) + (\varphi_h^I - \varphi_h)$ in (46), where φ_h^I denotes an interpolant of $\varphi \in W_h^\varphi$, to obtain

$$
\begin{aligned}
\int_0^T \int_\Omega |e||\psi|\, dx\, dt \leq\ & C \int_0^T \int_\Omega \Big|\epsilon \frac{\partial^2 E_h}{\partial t^2} + \nabla \times (\mu^{-1}\nabla \times E_h)- \\
& - s\nabla(\mu^{-1}\nabla \cdot E_h) + j + s\nabla(\nabla \cdot j))\Big| \cdot \Big|\varphi - \varphi_h^I\Big|\, dx\, dt+ \\
& + C \int_0^T \int_\Omega \epsilon \cdot \Big|\Big[\partial_{t_k}(\varphi - \varphi_h^I)\Big]\Big| \cdot \Big|E_h\Big|\, dx\, dt+ \\
& + C \int_0^T \int_\Omega \max_{S \subset \partial K} h_K^{-1}\frac{1}{\mu}\Big|\Big[E_h \times n\Big]\Big| \cdot \Big|\nabla \times (\varphi - \varphi_h^I)\Big|\, dx\, dt+ \\
& + C \int_0^T \int_\Omega \max_{S \subset \partial K} h_K^{-1}\frac{1}{\mu}\Big|\Big[E_h \cdot n\Big]\Big| \cdot \Big|\nabla \cdot (\varphi - \varphi_h^I)\Big|\, dx\, dt+ \\
& + C \int_0^T \int_\Omega \epsilon \cdot \Big|\Big[\partial_{t_k} E_h\Big]\Big| \cdot \Big|\varphi - \varphi_h^I\Big|\, dx\, dt+ \\
& + C \int_0^T \int_\Omega \max_{S \subset \partial K} h_K^{-1}\frac{1}{\mu}\Big|\Big[n \times \nabla \times E_h\Big]\Big| \cdot \Big|\varphi - \varphi_h^I\Big|\, dx\, dt+ \\
& + C \int_0^T \int_\Omega \max_{S \subset \partial K} h_K^{-1}\frac{1}{\mu}\Big|\Big[n \cdot (\varphi - \varphi_h^I)\Big]\Big| \cdot \Big|\nabla \cdot E_h\Big|\, dx\, dt.
\end{aligned}
\tag{47}
$$

By using standard interpolation estimates (36) for $\varphi - \varphi_h^I$ we conclude that:

$$
\begin{aligned}
\int_0^T \int_\Omega |e||\psi|\, dx\, dt \leq\ & C \int_0^T \int_\Omega \Big|\epsilon \frac{\partial^2 E_h}{\partial t^2} + \nabla \times (\mu^{-1}\nabla \times E_h)- \\
& - s\nabla(\mu^{-1}\nabla \cdot E_h) + j + s\nabla(\nabla \cdot j)\Big| \cdot \Big(\tau^2\Big|\frac{\partial^2 \varphi}{\partial t^2}\Big| + h^2\Big|D_x^2\varphi\Big|\Big)\, dx\, dt+ \\
& + C \int_0^T \int_\Omega \epsilon \cdot \Big[\partial\Big(\tau^2\Big|\frac{\partial^2 \varphi}{\partial t^2}\Big| + h^2\Big|D_x^2\varphi\Big|\Big)_t\Big] \cdot \Big|E_h\Big|\, dx\, dt+ \\
& + C \int_0^T \int_\Omega \max_{S \subset \partial K} h_K^{-1}\frac{1}{\mu}\Big|\Big[E_h \times n\Big]\Big| \cdot \Big(\nabla \times \Big(\tau^2\Big|\frac{\partial^2 \varphi}{\partial t^2}\Big| + h^2\Big|D_x^2\varphi\Big|\Big)\Big)\, dx\, dt+ \\
& + C \int_0^T \int_\Omega \max_{S \subset \partial K} h_K^{-1}\frac{1}{\mu}\Big|\Big[E_h \cdot n\Big]\Big| \cdot \Big(\nabla \cdot \Big(\tau^2\Big|\frac{\partial^2 \varphi}{\partial t^2}\Big| + h^2\Big|D_x^2\varphi\Big|\Big)\Big)\, dx\, dt+ \\
& + C \int_0^T \int_\Omega \epsilon \cdot \Big|\Big[\partial_{t_k} E_h\Big]\Big| \cdot \Big(\tau^2\Big|\frac{\partial^2 \varphi}{\partial t^2}\Big| + h^2\Big|D_x^2\varphi\Big|\Big)\, dx\, dt+ \\
& + C \int_0^T \int_\Omega \max_{S \subset \partial K} h_K^{-1}\frac{1}{\mu}\Big|\Big[n \times \nabla \times E_h\Big]\Big| \cdot \Big(\tau^2\Big|\frac{\partial^2 \varphi}{\partial t^2}\Big| + h^2\Big|D_x^2\varphi\Big|\Big)\, dx\, dt+ \\
& + s\,C \int_0^T \int_\Omega \max_{S \subset \partial K} h_K^{-1}\frac{1}{\mu}\Big[n \cdot \Big(\tau^2\Big|\frac{\partial^2 \varphi}{\partial t^2}\Big| + h^2\Big|D_x^2\varphi\Big|\Big)\Big] \cdot \Big|\nabla \cdot E_h\Big|\, dx\, dt.
\end{aligned}
\tag{48}
$$

In (48) the terms $\frac{\partial^2 E_h}{\partial t^2}, \nabla \times (\mu^{-1}\nabla \times E_h), \nabla(\mu^{-1}\nabla \cdot E_h)$ vanish because (E_h is continuous and piecewise linear). Finally, we use the estimates $\frac{\partial^2 \varphi}{\partial t^2} \approx \frac{\left[\frac{\partial \varphi_h}{\partial t}\right]}{\tau}$ and $D_x^2\varphi \approx \frac{\left[\frac{\partial \varphi_h}{\partial n}\right]}{h}$ to get the following a posteriori error representation formula:

Theorem 6.1. *Let φ be the solution to (39), E the solution of (12), and E_h the FEM approximation of E. Then the following error representation formula holds:*

$$\int_0^T \int_\Omega |e||\psi| \; dx \; dt \leq \int_0^T \int_\Omega R_1\sigma_1 \; dx \; dt+$$

$$+ \sum_k \int_\Omega R_2\sigma_2 \; dx + \int_0^T \int_\Omega R_3\sigma_3 \; dx \; dt+$$

$$+ \int_0^T \int_\Omega R_4\sigma_4 \; dx \; dt + \sum_k \int_\Omega R_5\sigma_1 \; dx+ \tag{49}$$

$$+ \int_0^T \int_\Omega R_6\sigma_1 \; dx \; dt + \int_0^T \int_\Omega R_7\sigma_5 \; dx \; dt,$$

where the residuals are defined by

$$R_1 = \left|j + s\nabla(\nabla \cdot j)\right|, \;\; R_2 = \epsilon\left|E_h\right|, \;\; R_3 = \max_{S \subset \partial K} h_K^{-1}\frac{1}{\mu}\left|\left[E_h \times n\right]\right|,$$

$$R_4 = \max_{S \subset \partial K} h_K^{-1}\frac{1}{\mu}\left|\left[E_h \cdot n\right]\right|, \;\; R_5 = \epsilon\left|\left[\partial_{t_k}E_h\right]\right|,$$

$$R_6 = \max_{S \subset \partial K} h_K^{-1}\frac{1}{\mu}\left|\left[n \times \nabla \times E_h\right]\right|, \;\; R_7 = \max_{S \subset \partial K} h_K^{-1}\frac{1}{\mu}\left|\nabla \cdot E_h\right|, \tag{50}$$

and the interpolation errors are

$$\sigma_1 = C\tau\left|\left[\frac{\partial \varphi_h}{\partial t}\right]\right| + Ch\left|\left[\frac{\partial \varphi_h}{\partial n}\right]\right|,$$

$$\sigma_2 = C\left[\partial\left(\tau\left|\left[\frac{\partial \varphi_h}{\partial t}\right]\right| + h\left|\left[\frac{\partial \varphi_h}{\partial n}\right]\right|\right)_t\right],$$

$$\sigma_3 = C \; \nabla \times \left(\tau\left|\left[\frac{\partial \varphi_h}{\partial t}\right]\right| + h\left|\left[\frac{\partial \varphi_h}{\partial n}\right]\right|\right), \tag{51}$$

$$\sigma_4 = C \; \nabla \cdot \left(\tau\left|\left[\frac{\partial \varphi_h}{\partial t}\right]\right| + h\left|\left[\frac{\partial \varphi_h}{\partial n}\right]\right|\right),$$

$$\sigma_5 = C \; \left[n \cdot \left(\tau\left|\left[\frac{\partial \varphi_h}{\partial t}\right]\right| + h\left|\left[\frac{\partial \varphi_h}{\partial n}\right]\right|\right)\right].$$

6.2. **Adaptive algorithm.** The main goal in adaptive error control is to find a mesh K_h with as few number of nodes as possible, such that $||E - E_h|| < tol$. Clearly, we cannot find E analytically. Instead, using the a posteriori error estimate in Theorem 1, we shall find a triangulation K_h, such that the corresponding finite element approximation E_h satisfies

$$R_1 \cdot \sigma_1 + R_2 \cdot \sigma_2 + R_3 \cdot \sigma_3 + R_4 \cdot \sigma_4 + R_5 \cdot \sigma_1 + R_6 \cdot \sigma_1 + R_7 \cdot \sigma_5 < tol. \tag{52}$$

The solution is found by an iterative process, where we start with a coarse mesh and successively refine the mesh by using the stopping criterion (52) with as few number of elements as possible. More precisely, in the computations below we shall use the following

Adaptive algorithm

1. Choose an initial mesh K_h and an initial time partition J_τ of the time interval $[0, T]$.
2. Compute the solution E^n of (12) on K_h and J_τ.
3. Compute the solution φ^n of the adjoint problem (39) on K_h and J_τ.
5. Construct a new mesh K_h and a new time partition J_k of the time interval $(0, T)$ using a posteriori error estimate of Theorem 1. More precisely, refine all elements, where $R_1 \cdot \sigma_1 + R_2 \cdot \sigma_2 + R_3 \cdot \sigma_3 + R_4 \cdot \sigma_4 + R_5 \cdot \sigma_1 + R_6 \cdot \sigma_1 + R_7 \cdot \sigma_5 > tol$. Here tol is a

tolerance chosen by the user. Return to 1. On J_k the new time step τ should satisfy CFL condition.

Remark During the refinement procedure we do not allow the appearance of new nodes inside the overlapping layers. In the case of the presence of parameters ϵ and μ in equation (12) we interpolate them after every refinement on a new refined mesh. We also need impose compatibility conditions for these coefficients in the case of non-smooth material interfaces to avoid discontinuities for these coefficients. In this case ϵ and μ should be replaced with smooth functions ϵ_1 and μ_1.

7. NUMERICAL EXAMPLES

We have implemented our adaptive hybrid FEM/FDM method in C++, with different modules handling the finite elements, the finite differences, and the communication required for the coupling. The software packages PETSc [4] and MV++ [33] are used for matrix-vector computations. All our computations (2D and 3D) were performed on a standard high-end workstation (3.2 GHz Intel Xeon$^{\text{TM}}$ processor, 2Gb RAM and 2Mb L3 cache). We shall now evaluate the performance of our hybrid FEM/FDM method in two and three dimensions.

7.1. **Two dimensional examples.** The computational domain is $\Omega = [0.2, 0.8]^2$; it separates into a finite element domain, $\Omega_{FEM} = [0.4, 0.6]^2$, and a surrounding finite difference domain Ω_{FDM}. In all computations we choose the time step τ according to the CFL condition (30), while the penalty factor in (16) is always set to $s = 1$.

In the following examples we consider a plane wave $E = (0, E_2)$, given by

$$E_2(x, y, t) \mid_{y=0} = (\sin(5(t - 2\pi/5) - \pi/2) + 1)/10, \quad 0 \leq t \leq \frac{2\pi}{5}, \tag{53}$$

which initiates at the lower boundary of Ω_{FDM} and propagates upwards.

To validate the implementation and show the convergence of our hybrid method, we first consider (12) with $\epsilon = \mu = 1.0$ and $j = 0$. Hence, the electromagnetic field consists of the plane wave given as in (53). At the lateral boundaries we use periodic boundary conditions, and at the top boundary first-order absorbing boundary conditions [11], which is exact in this particular case. We compute the maximal error $e = \max_{[0,T]} \left| E_{ref} - E_h \right|$, where E_{ref} denotes the reference solution computed on the finest mesh with 25921 nodes and 51200 elements, and E_h denotes the solution computed on the sequence of adaptively refined meshes shown in Table 1. All integrals are computed over the inner domain Ω_{FEM}, which remains fixed during the entire computation and at all refinement steps. Note that every node on any intermediate mesh coincides with some node on the finest mesh; hence, we never need to interpolate E_{ref} on coarser meshes.

Table 2 and Figure 5 illustrates the convergence behavior of the FEM-solution in the hybrid method compared with Yee scheme as the mesh is refined. Both the error in the FEM-solution and that obtained by using the Yee scheme everywhere in Ω on an equidistant mesh are shown. As expected, both methods are second-order convergent, with the Yee scheme slightly more accurate than the FE scheme for a comparable mesh size.

Next, we shall demonstrate the continuity of the numerical solution across the FD/FE mesh in the presence of material discontinuities. To do so, we consider the same problem as above, with $\epsilon = \mu = 1.0$ outside the ellipse shown in Fig. 4, and either $\epsilon = 20, \mu = 1.0$ or $\epsilon = \mu = 20$ inside. As shown in Fig. 6, the isolines of the solutions remain smooth both across the FE/FD interface and material jumps.

7.2. **Three dimensional examples.** Next, we consider (12) in $\Omega = [0, 5.1] \times [0, 2.5] \times [0, 2.5]$, which is divided into a finite element domain $\Omega_{FEM} = [0.3, 4.7] \times [0.3, 2.3] \times [0.3, 2.3]$, with an unstructured tetrahedral mesh, and a surrounding finite difference domain Ω_{FDM}, with a structured hexahedral mesh with mesh size $h = 0.2$. First order absorbing boundary conditions are imposed at all boundaries of Ω_{FDM} and the final time is $T = 3.0$. Here, the electromagnetic

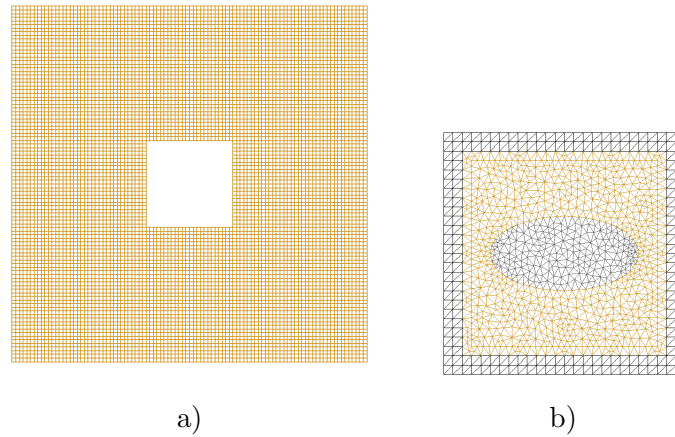a)   b)

FIGURE 4. Computational mesh in two dimensions. The hybrid mesh (c) is a combination of the structured mesh Ω_{FDM} (a) and the unstructured mesh Ω_{FEM} (b) with a thin overlap of structured elements.
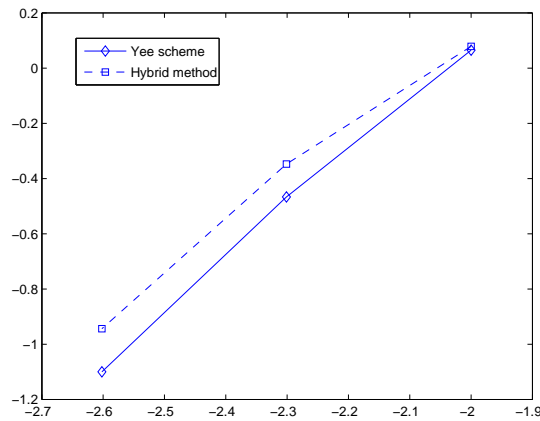

FIGURE 5. Convergence of L_2 error in space and time for Yee scheme and hybrid method.

field consists of a spherical wave, generated at the point $x_0 = (2.05, 2.2, 1.25)$ in Ω_{FEM} by the source term

$$f_1(x, x_0) = \begin{cases} 10^3 \sin^2 \pi t & \text{if } 0 \leq t \leq 0.1 \text{ and } |x - x_0| < 0.1, \\ 0 & \text{otherwise.} \end{cases} \tag{54}$$

The material parameters are $\epsilon = 2.0$ and $\mu = 1.0$ inside the cube, and $\epsilon = \mu = 1.0$ everywhere else. In Fig. 7 we show the isosurfaces of the numerical solutions inside Ω_{FEM} at different times.

We now use the results from the a posteriori error analysis in Section 6 to estimate the error in the numerical solution of (12). According to Theorem 1 the error bound consists of space-time integrals of different residuals multiplied by the solution of the dual problem. The residuals indicate how well the numerical solution satisfies the differential equation, whereas the solution of the dual problem determines how the error propagates through space and time. Thus, to estimate the error in the numerical solution, we need to compute an approximate solution of the dual problem together with the residuals. Since the residuals R_1, R_2, R_5 and weights dominate, we neglect the terms I_3, I_4, I_6, I_7 in the a posteriori error estimator.

h	No_{nodes} in Ω_{FEM}	$No_{elements}$ in Ω_{FEM}	No_{nodes} in Ω	$No_{elements}$ in Ω
0.025	81	128	625	640
0.02	121	200	961	1000
0.01	441	800	3721	4000
0.005	1681	3200	14641	16000
0.0025	6561	12800	58081	64000
0.00125	25921	51200	231361	256000

TABLE 1. Computational meshes in two dimensions.

h	$\max_{[0,T]}\left|E_{ref} - E_h\right|$	$\max_{[0,T]}\left|E_{ref} - E_h\right|$
0.01	1.19879	1.16128
0.005	0.449274	0.341658
0.0025	0.113817	0.0794665

TABLE 2. Error in time over the time interval $[0; 2.0]$: hybrid method (left) and Yee scheme (right).

Different choices for ψ as data in the dual problem yield a posteriori error estimates in different quantities of interest. Since we wish to control the error only in the finite element domain, we choose $\psi = 0$ in Ω_{FDM} and $\psi = 1$ in Ω_{FEM} which acts during the time interval $[1.55, 3.0]$, and $\psi = 0$ everywhere else and at all remaining times. To evaluate the effectiveness of the error estimator we now solve the dual problem (39) backward in time, that is from $T = 3.0$ down to $T = 0.0$, with $\epsilon = 20, \mu = 1$ inside the cube, and $\epsilon = \mu = 1$ elsewhere. In Fig. 8-a we show the L_2-norms in space of the solutions to the dual problem versus time for a sequence of adaptively refined meshes.

To compare the behavior of the solution to the dual problem at different times, we show in Fig. 8-b L_2-norms in space of φ when we solve problem (39) from $T = 6.0$ down to $T = 0.0$. We observe, that the solution of the dual problem grows backward in time through the action of ψ, but is reduced as the mesh is adaptively refined. In Fig. 9-a), one of the main components of the interpolation errors (51) in the a posteriori error estimator, $\left|\left|\left[\frac{\partial \varphi_h}{\partial t}\right]\right|\right|_{L_2}$, is shown on the time interval $[0.0, 2.0]$. We note that the jump in time of the dual solution is reduced on the adaptively refined meshes, as expected. The L_2-norm in space of the residual R_2, shown during the time interval $[0.0, 2.0]$ in Fig. 9-b), does not grow with time. Therefore, here the main error indicator is provided by the solution of the dual problem.

In Fig. 10 the highest value isosurfaces of the solution to the dual problem on a locally refined mesh is shown. We observe that isosurfaces are concentrated around the cube where the main error is located, precisely where local refinement is required. Then we construct a new mesh as described in Section (6.2), choose a new time step that satisfies the CFL condition, and return to step 1 in algorithm (6.2).

8. CONCLUSIONS

We have devised an explicit, adaptive, hybrid FEM/FDM method for the time dependent Maxwell equations. The method is hybrid in the sense that different numerical methods, finite elements and finite differences, are used in different parts of the computational domain. Inside the FE part of the computational domain, the adaptivity is based on a posteriori error estimates in the form of space-time integrals of residuals multiplied by dual weights. Their usefulness for adaptive error control is illustrated in three-dimensional numerical examples, where we solve

both the direct and the dual problems and compute the corresponding residuals and weights. In particular, our numerical examples show that by combining a divergence penalty term with adaptive mesh refinement, we eliminate spurious eigenmodes in time dependent calculations and achieve an accuracy close to that of the FDTD scheme on a comparable mesh.

The adaptive hybrid method combines the simplicity and speed of the FDTD scheme [40] on the structured part of the mesh with the flexibility of a FEM on the unstructured part of the mesh. Efficiency is obtained by using a fully explicit hybrid FEM/FDM method with optimized numerical linear algebra and adaptivity. Thus, we have developed a fast solver, which can be applied to the solution of computationally demanding problems, such as inverse electromagnetic problems in the time domain.

9. Acknowledgements

References

[1] Assous, F., Ciarlet, P., Sonnendrcker, Jr. and E., (1998), Resolution of the Maxwell's equations in a domain with reentrant corners, Math. Model. Num. Anal., 32, pp.359–389

[2] Assous, F., Ciarlet, P., Segre, Jr. and J., (2000), Numerical solution to the time-dependent Maxwell equations in two-dimensional singular domains: the singular complement method", J. Comput. Phys., 161, pp.218–249.

[3] Assous, F., Degond, P., Heintze E. and Raviart, P., (1993), On a finite-element method for solving the three-dimensional Maxwell equations, J.Comput.Physics, 109, pp.222–237.

[4] Balay, S., Gropp W. and McInnes, L-C., PETSc user manual, http://www.mcs.anl.gov/petsc.

[5] Bergstrm, R., (2002), Least-squares finite element methods with applications in electromagnetics, 10, Chalmers University of Technology, Sweden.

[6] Brenner, S. C., Scott, L. R., (1994), The Mathematical theory of finite element methods, Springer-Verlag.

[7] Cangellaris, A. C., Wright, D. B., (1991), Analysis of the numerical error caused by the stair-stepped approximation of a conducting boundary in FDTD simulations of electromagnetic phenomena, IEEE Trans.Antennas Propag., 39, pp.1518–1525.

[8] Bonnet-Ben Dhia, A. S., Hazard, C. and Lohrengel, S., (1999), A singular field method for the solution of Maxwell's equations in polyhedral domains, SIAM J. Appl. Math., 59-6, pp. 2028–2044.

[9] Edelvik, F., Andersson, U. and Ledfelt, G., (2000), Explicit hybrid time domain solver for the Maxwell equations in 3D, AP2000 Millennium Conference on Antennas & Propagation, Davos.

[10] Edelvik, F. and Ledfelt, G., (2000), Explicit hybrid time domain solver for the Maxwell equations in 3D., J. Sci. Comput.

[11] Elmkies, A. and Joly, P., (1997), Finite elements and mass lumping for Maxwell's equations: the 2D case, Numerical Analysis, C. R. Acad.Sci.Paris, 324, pp. 1287–1293.

[12] Engquist, B. and Majda, A., (1977), Absorbing boundary conditions for the numerical simulation of waves *Math. Comp.* **31**, pp.629-651

[13] Eriksson, K., Estep, D. and Johnson, C., (1996), Computational Differential Equations, Studentlitteratur, Lund.

[14] Eriksson, K., Estep, D., and Johnson, C., (1995), Introduction to adaptive methods for differential equations, Acta Numerica, Cambridge University Press, pp.105–158.

[15] Hansbo, P., and Johnson, C., (1998), Adaptive finite element methods for elastostatic contact problems, IMA Volumes in Mathematics and its Applications, 113, pp.135 –150.

[16] Hoffman, J. and Johnson, C., (2003), Dynamic computational subgrid modelling, Lecture Notes in Computational Science and Engineering, Springer.

[17] Hughes, T. J. R., (1987), The finite element method, Prentice Hall.

[18] Hwang, C. T. and Wu, R. B., (1999), Treating late-time instability of hybrid finite-element/finite difference time-domain method, IEEE Trans. Antennas Propag., 47, pp.227–232.

[19] Jiang, B., (1998), The Least-Squares Finite Element Method, Theory and Applications in Computational Fluid Dynamics and Electromagnetics, Springer-Verlag, Heidelberg.

[20] Jiang, B., Wu, J. and Povinelli, L. A., (1996), The origin of spurious solutions in computational electromagnetics, J. Comput. Phys., 125, pp.104–123.

[21] Jin, J., (1993), The finite element method in electromagnetics, Wiley.

[22] Johnson, C., (2000), Adaptive computational methods for differential equations, ICIAM99, Oxford University Press, pp.96–104.

[23] Joly, P., (2003), Variational methods for time-dependent wave propagation problems, Lecture Notes in Computational Science and Engineering, Springer.

[24] Lee, R. L. and Madsen, N. K., (1990), A mixed finite element formulation for Maxwell's equations in the time domain, J. Comput. Phys., 88, pp.284–304.

[25] Monk, P. B., (2003), Finite Element methods for Maxwell's equations, Oxford University Press.

[26] Monk, P. B. and Parrott, A. K., (1994), A dispersion analysis of finite element methods for Maxwell's equations, SIAM J.Sci.Comput., 15, pp.916–937.

[27] Monk, P. B., (1992), A comparison of three mixed methods, J.Sci.Statist.Comput., 13.

[28] Monorchio, A. and Mittra, R., (1998), A Hybrid Finite-Element Finite-Difference Time-Domain Technique for Solving Complex Electromagnetic Problems, IEEE Microwave and Guided Wave Letters, 8, pp.93–95.

[29] Munz, C. D., Omnes, P., Schneider, R., Sonnendrcker, E. and Voss, U., (2000), Divergence correction techniques for Maxwell Solvers based on a hyperbolic model, J.of Comp.Phys., 161, pp.484–511.

[30] Mur, G., (1998), The fallacy of edge elements, IEEE Trans. Magnetics, 34(5), pp.3244–3247.

[31] Nédélec, J.C., (1986), A new family of mixed finite elements in $\mathbb{R}^3$, NUMMA, 50, pp.57–81.

[32] Paulsen, K. D., Lynch, D. R., (1991), Elimination of vector parasities in Finite Element Maxwell solutions, IEEE Trans.Microwave Theory Tech.,39, pp. 395-404.

[33] R. Pozo, MV++ user manual, http://math.nist.gov/mv++/

[34] Rylander, T., Bergstrm, R., Levenstam, M., Bondeson, A.,Johnson, C., (1998), FEM algorithms for Maxwell's equations, Electromagnetic Computations for Analysis and Design of Complex Systems, EMB 98, Linkping, Sweden.

[35] Rylander, T. and Bondeson, A., (2000), Stable FEM-FDTD hybrid method for Maxwell's equations, J. Comput.Phys.Comm., 125 p.

[36] Rylander, T. and Bondeson, A., (2002), Stability of Explicit-Implicit Hybrid Time-Stepping Schemes for Maxwell's Equations, J. Comput.Phys.

[37] Taflove, A., (1998), Advances in Computational Electromagnetics: The Finite Difference Time-Domain Method, Boston, MA:Artech House.

[38] Wu, R. B., Itoh, T., (1997), Hybrid finite-difference time-domain modeling of curved surfaces using tetrahedral edge elements, IEEE Trans.Antennas Prop., 45, pp.1302-1309.

[39] Wu, R. B., Itoh, T., (1995), Hybridizing FDTD analysis with unconditionally stable FEM for objects of curved boundary, IEEE MTT-S Dig., 2, pp.833-836.

[40] Yee, K. S., (1966), Numerical solution of initial boundary value problems involving Maxwell's equations in isotropic media, IEEE Trans. Antennas Propag.,14, pp.302-307.

a) $t = 1.3$ b) $t = 1.3$

c) $t = 2.3$ d) $t = 2.3$

e) $t = 2.9$ f) $t = 2.9$
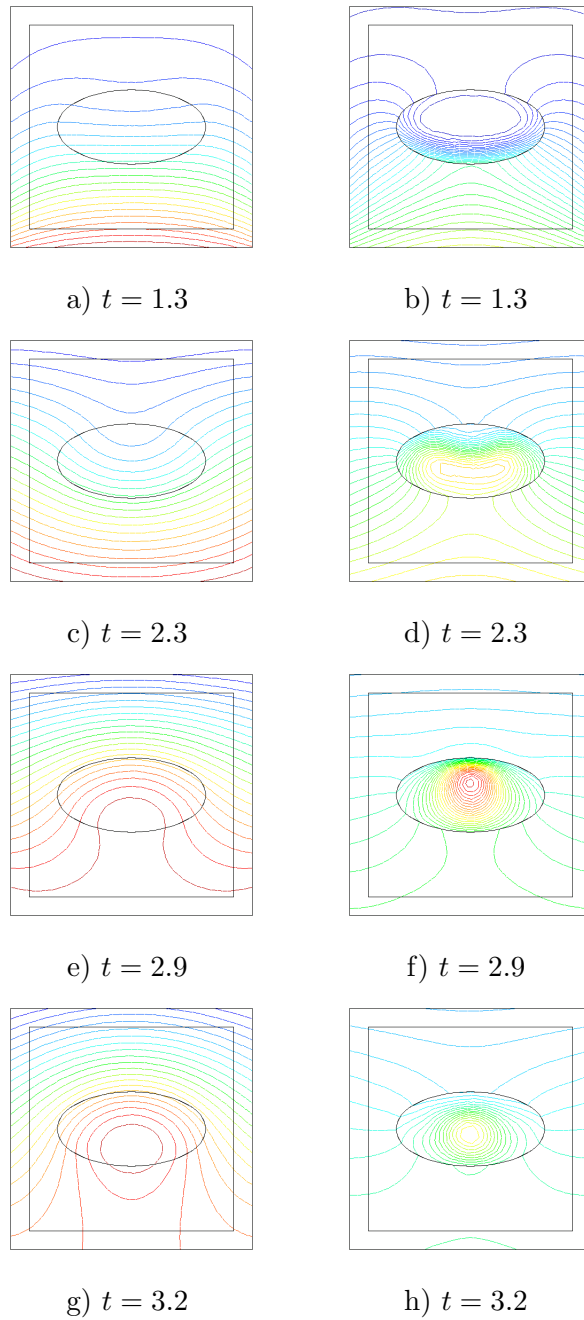
g) $t = 3.2$ h) $t = 3.2$

FIGURE 6. Isolines of the computed solution in hybrid method for geometry, presented in Fig. 4, with different values of the parameters ϵ, μ: in a), c), e), g) $\epsilon = 20, \mu = 1$ inside the ellipse, whereas in b), d), f), h) $\epsilon = \mu = 20$ inside the ellipse. In both cases $\epsilon = \mu = 1$ everywhere else in Ω.

a) $t = 0.3$ b) $t = 1.2$

c) $t = 0.7$ d) $t = 1.5$
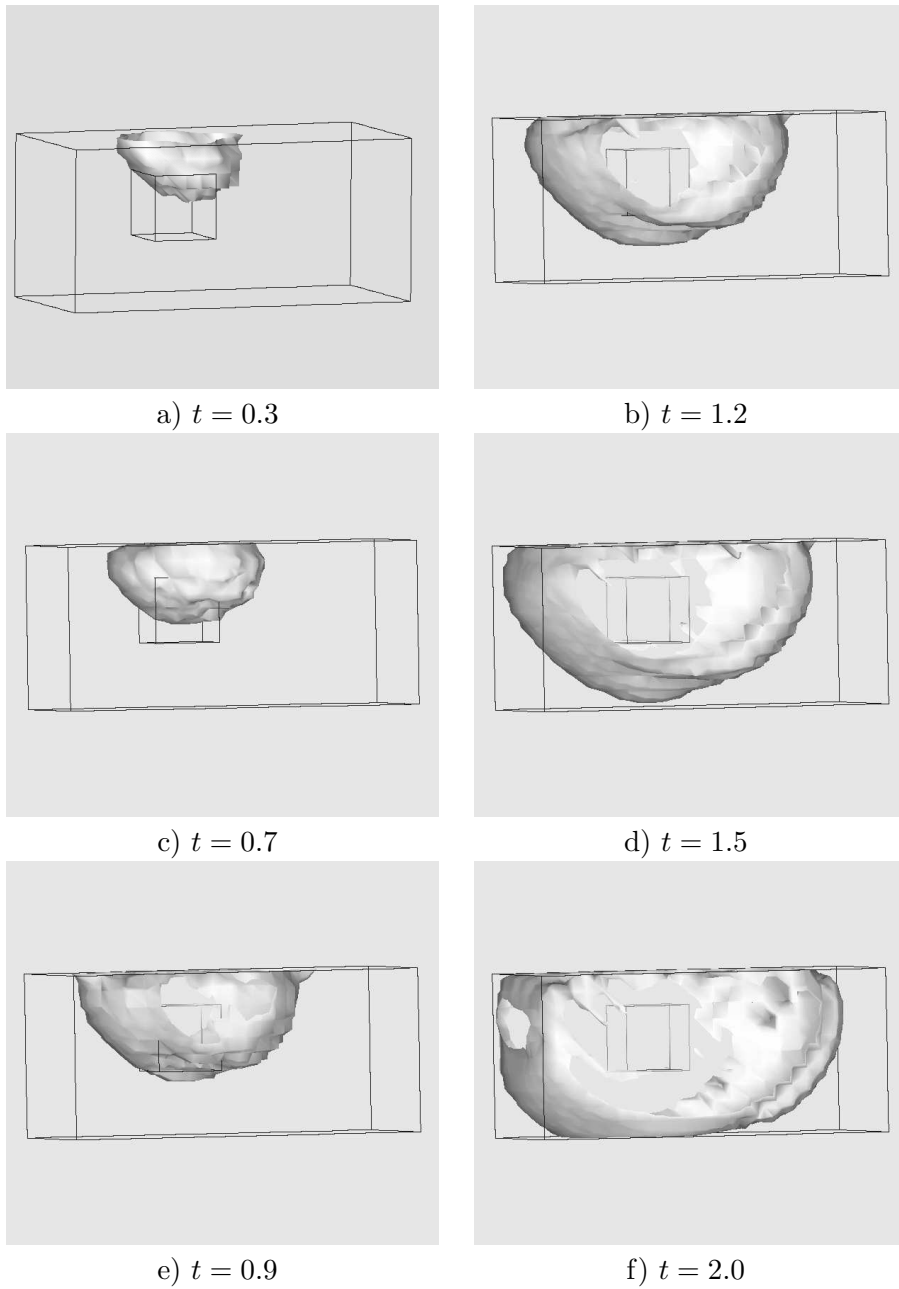
e) $t = 0.9$ f) $t = 2.0$

FIGURE 7. Solution of problem (12) in Ω_{FEM} with one spherical pulse. We present isosurfaces at different time moments. Values $\epsilon = 2.0, \mu = 1.0$ are inside the cube, and $\epsilon = 1.0, \mu = 1.0$ everywhere else in Ω.
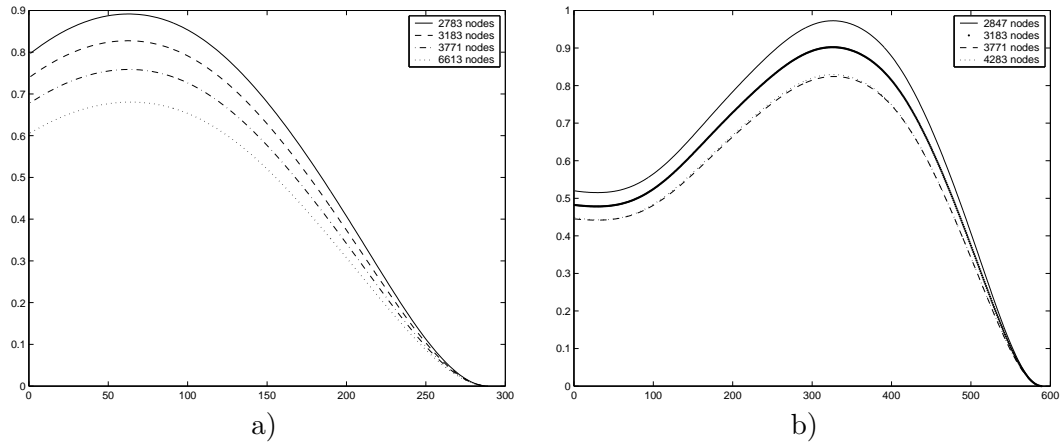
FIGURE 8. $|\varphi|_{L_2}$ for problem (39) on adaptively refined meshes during the time interval $[0, 3.0]$ (a) and $[0, 6.0]$ (b).
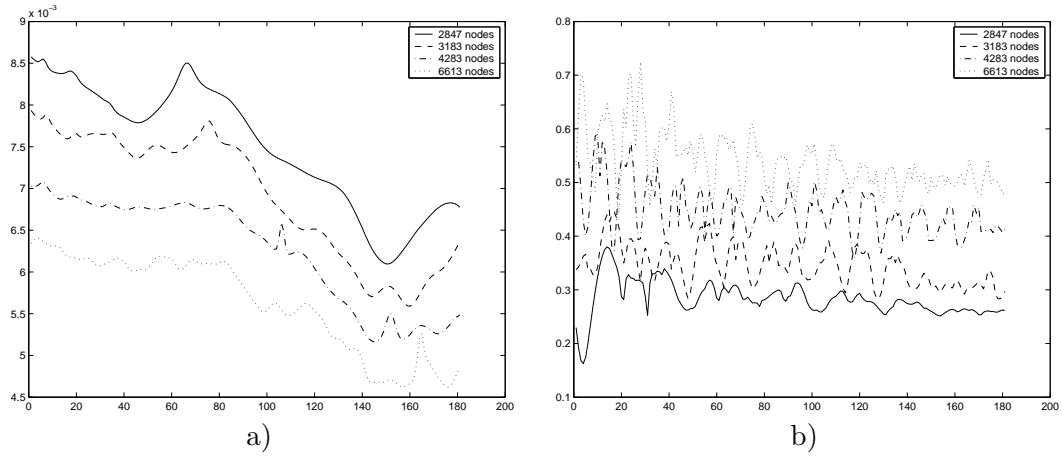

FIGURE 9. L_2-norms in space on adaptively refined meshes : a) $\left[\frac{\partial \varphi_h}{\partial t}\right]$, b) $[E_{h_t}]$.
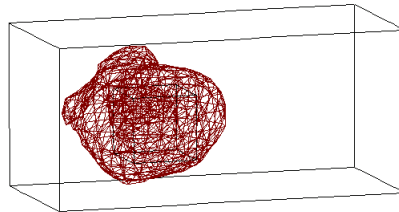

FIGURE 10. The highest value isosurface of the dual solution φ.

Since 2009 **L.Beilina** works as an Associate Lecturer at the Department of Mathematical Sciences at Chalmers University of Technology and Gothenburg University, Sweden. She obtained her Ph.D. in Applied Mathematics in 2003 at the same department. After that in 2003-2005 she worked as an Assistant Professor at the Department of Mathematics, University of Basel, Switzerland, and in 2007-2008 - as an Assistant Professor at the Department of Mathematical Sciences at NTNU, Trondheim, Norway.

Since 2001 **Marcus J. Grote** is a Professor of Numerical Analysis and Computational Mathematics at the Department of Mathematics, University of Basel, Switzerland. He obtained his Ph.D. in Scientific Computing and Computational Mathematics in 1995 at Stanford University, USA. After that in 1995-1997 he was associate research scientist at the Courant Institute of Mathematical Sciences, New-York, USA, and in 1997-2001 he worked as an Assistant Professor at the Department of Mathematics in ETH, Zurich, Switzerland.